Determination of Interfacial Tension of binary n mixtures of n–alkanes $+ CH_4$ and $n-$ alkanes $+ CO_2$ using Density gradient theory and Peng-Robinson Equation of State at elevated temperatures and pressures

Abstract: The interfacial tensions of alkanes in the presence ofCH_4 and CO_2 were predicted using the model taken as a combination of Density Gradient theory and Peng-Robinson equation of state and compared with existing simulation data. The main aim of this work was to make a progress in modeling the IFTs between diverse n-alkanes and CH_4andCO_2 natural gases. Several statistical measures and graphical descriptions were employed to aid the accuracy analysis of the proposed model. The statistical measures indicate a complex relationship among thermal conditions, model selection, and performance metrics, which can be observed by examining the tables presented in this work. Overall, the results indicate that the Peng-Robinson equation effectively predicted the interfacial tensions.

Keywords: Density gradient theory; Interfacial tension; n-alkanes; Natural gases and Statistical errors.

1. Introduction

Numerous experimental, theoretical, and simulation investigations have been conducted on the interfacial characteristics of binary mixtures of n-alkane with natural gases such asCH_4 and CO_2 in different ranges of temperature and pressure [Mahdaviara et al. 2021; Li et al. 2017; Menand et al., 2020; Mique et al.,2008; Carey et al., 1980; Ameli et al., 2018; Laffite et al., 2006; Amezquita et al., 2010; Hough et al., 1961; Choudhary et al., 2019; Mirzaie et al., 2020, Amar et al., 2021].Several authors have sought to estimate this parameter to circumvent the complexities and expenses linked to laboratory measurements. In recent decades, various mathematical and thermodynamic models have emerged as promising approaches for interfacial tension (IFT) estimation, including the Parachor [Macleod et al., 1923; Sugden et al., 1924], Scaling Law Method [Mique et al.,(2008); Guggenheim et al.,1945]Corresponding State Method [Mique et al., 2008; Zuo et al., 1996; Guggenheim et al., 1945], Linear Gradient Theory (DGT)[Mique et al., 2008; Pereira et al., 2016] and Density Gradient Theory (DGT) [Mique et al., 2008; Aahrafizadeh et al., 2011]. Additionally, several researchers have utilized combinations of these theoretical models along with different Equations of State (EOSs) to concurrently clarify various interfacial properties of fluid systems in the presence of different gases. Some simulation methods, such as Molecular Dynamic(MD) simulations [Choudhary et al., 2021], have been

also found as useful approaches for addressing the IFT of the diverse systems. To our knowledge, only a limited number of -experimental investigations [Choudhary et al., 2021; Mejia et al., 2014; Jaeger et al., 2010; Miquez et al., 2014; Mirzaie et al., 2020; Mahdaviara et al., 2022; Zolghadr et al., 2013] examining the interfacial tension of (n-alkanes+CH_4) and (n-alkanes +CO_2) systems have been conducted at the pressure conditions considered in this study. In the paper they [Choudhary et al., 2021] have utilized volume translated Peng-Robinson equation of state(VT-PR EOS) for prediction of interfacial tension at these pressures. The van der Waals theory is the foundation of density gradient theory for inhomogeneous fluids. It was rediscovered by Cahn and Hilliard [Cahn & Hilliard 1958] and represents an extension of the Helmholtz free energy density around a step density profile that is truncated after the second term. The local free energy density is calculated using an equation of state, such as the Peng-Robinson equation.

2. Density gradient theory

The density gradient theory (DGT) [Cahn & Hilliard et al., 1958; Li et al., 2008; Mejia et al., 2014; Carey et al., 1980; Mique et al., 2004] is based on a mean field approximation that describes the uniform evolution of Helmholtz energy density across the interface. This approach aids in determining interfacial parameters, such as the density profile and interfacial tension. Sahimi [Sahimi et al., 1991] confirmed the DGT to be more efficient and precise than other methods. This technique primarily uses the equation of state (EOS) to analyze interfacial characteristics and phase equilibrium. The DGT has been combined with various equations of state. Cahn and Hilliard developed the well-known equation, which describes the separation of phases in binary alloys. Since its inception, the CH equation has been applied across numerous fields, including science, chemistry, physics, and biology. Consequently, understanding how this equation operates within different models is essential. Currently, density gradient theory serves as an effective method for determining the interfacial tension of mixtures. Understanding the influence parameter is essential for computation. Assume the interface between the liquid and vapor bulk phases is planar. The interface thickness is represented by z, which denotes the distance normal to this interface. According to the density gradient theory, in the absence of external potentials, the differential equation governing the density distributions $\rho_i(z)$through a planar interface is given by equation (1) [Reno et al., 1943; Hough et al., 1961; Ameli et al., 2018; Blas et al., 2001]. In this context, n_c represents the number of components in the mixture, and $\Omega(\rho)$ represents the grand thermodynamic potential.

$$\sum_{j=1}^{n_c} \frac{d}{dz}\left(c_{ij}\frac{d\rho_j}{dz}\right) - \frac{1}{2}\sum_{j=1}^{n_c}\sum_{k=1}^{n_c}\frac{\partial c_{jk}}{\partial \rho_i}\frac{d\rho_j}{dz}\frac{d\rho_k}{dz} = \frac{\partial \Omega(\rho)}{\partial \rho_i} \tag{1}$$

The information regarding the intermolecular geometry of the interface is encapsulated within the influence parameter. This parameter also establishes a link between the extent of deviation in the Helmholtz energy density and the chemical potential. The grand thermodynamic potential, represented by the symbol $\Delta\Omega(\rho)$, is defined as follows:

$$\Delta\Omega(\rho) = f^0(\rho) - \sum_i \rho_i \mu_i^B + P \tag{2}$$

where$f^0(\rho)$ is the local Helmholtz free energy of homogeneous fluid at interfacial region of density$\rho_i(z)$ whereasμ_i^B the chemical potential of component *i* in the bulk phase. In equation (1), the second component of

the left-hand side (L.H.S.) will not be present when considering that the influence parameter c_{jk} are independent of composition. This allows for the simplification of the governing equation (1) for the planar interface to

$$\sum_{j=1}^{n_c} c_{ij} \frac{d^2\rho_i}{dz^2} = \mu_i(\rho) - \mu_i^B \tag{3}$$

where the $\mu_i(\rho)$ is the chemical potential at the interfacial region where the density equals to ρ. Multiplying equation(3) by $d\rho_i/dz$, summing over i and integrating gives

$$\sum_i \sum_j \frac{1}{2} c_{ij} \frac{d\rho_i}{dz} \frac{d\rho_j}{dz} = \Delta\Omega(\rho) - \Phi^B \tag{4}$$

Equation (4) describes the difference between the grand thermodynamic potential $\Delta\Omega(\rho) = f^0(\rho) - \sum_i \rho_i \mu_i^B$ at local composition and its corresponding value in the bulk phases, which is denoted as $\Phi^B = -P$, where *P* represents the vapor-liquid equilibrium pressure. The differential equation (3) is governed by the following boundary condition $z \to +\infty, \rho \to \rho^L$

$$z \to -\infty, \rho \to \rho^V$$

where theρ^L and ρ^V are the liquid and vapor phase densities. Using gradient theory, the interfacial tension is computed as:

$$\int_{\rho^V}^{\rho^L} \left(2(\Phi(\rho) - \Phi^B) \sum_i \sum_j c_{ij} \frac{d\rho_i}{d\rho} \frac{d\rho_j}{d\rho} d\rho \right. \tag{5}$$

The equilibrium pressure (P), Helmholtz free energy density (f^0), and chemical potential (μ_i) at the interface can be calculated. Now, the density profiles can be obtained from the following expression

$$z = z_0 + \int_{\rho^V}^{\rho^L} \sqrt{\frac{\sum_i \sum_j c_{ij} \frac{d\rho_i}{d\rho} \frac{d\rho_j}{d\rho}}{2\Delta\Omega(\rho)}} d\rho$$

wherez_0 is an arbitrarily chosen position.

Here we have utilized the Peng-Robinson equation of state [Mejia et al., 2014; Choudhary et al., 2021] to calculate the densities ρ^L and ρ^V in the liquid and vapor phase in equilibrium.

$$P = \frac{RT}{v-b} - \frac{a(T)}{v(v+b)+b(v-b)}$$

Carey and co workers [Carey et al., 1980] were the first to offer such a combination of the gradient theory and PR-EOS, and since then, it has been adopted on multiple times in the literature.

This study employs the classical van der Waals mixing rules for the co-volume parameter b and the temperature-dependent energy parameter $a(T)$of the mixture:

$$b = \sum_i x_i b_i \tag{6}$$

$$a = \sum_i \sum_j x_i x_j (1 - k_{ij}) \sqrt{a_i a_j} \tag{7}$$

wherex_i are the mole fractions of component$i$ in each phase and are the binary interaction parameters.The parameter of pure fluids are defined by classical equations

$$b_i = 0.07780\frac{RT_{c_i}}{P_{c_i}} \quad (8)$$

$$a_i(T) = 0.45724\frac{R^2T_{c_i}^2}{P_{c_i}}\alpha\left(T_{r_i}\right) \quad (10)$$

with

$$\alpha\left(T_{r_i}\right) = \left\{1 + m_i\left(1 - \sqrt{T_{r_i}}\right)\right\}^2 \quad (11)$$

Table 7 gives the critical properties and acentric factor for alkanes and gases used in equations (8) to (11).

3. Influence parameter

According to the mixing rule, the pure component influence parameters c_i and $c_j$are connected to the cross influence parameters:

$$c_{ij} = \left(1 - \beta_{ij}\right)\sqrt{c_i c_j} \quad (11)$$

whereβ_{ij} are binary interaction coefficients. For thermodynamic stability of the interface, the values β_{ij} must be constrained between 0 and 1. The mixing rule is simplified to the geometric mean. Previous literature indicates that the geometric mixing rule for influence parameters provides the most efficient estimation for hydrocarbon/hydrocarbon pairs and gas (carbon dioxide, methane, or nitrogen)/hydrocarbon pairs. The expression for the influence parameter applicable to non-polar pure fluids is determined when the gradient theory is combined with the PR-EOS. It describes the variation of the influence parameter with the reduced temperature $t_i = 1 - T/T_{c_i}$ as follows:

$$\frac{c_i}{a_i b_i^{2/3}} = A_i t_i + B_i$$

where$b_i$is the co-volume anda_i is the energy parameter in the PR-EOS. The coefficients $A_i$and $B_i$are only associated with the acentric factor of the component i by the relationships:

$$A_i = \frac{-10^{-16}}{1.2326 + 1.377\omega_i} \quad (13)$$

$$B_i = \frac{-10^{-16}}{0.9051 + 1.5410\omega_i} \quad (14)$$

To compute interfacial tension values using equation (5), estimate the density distribution of each component($d\rho_i/dz$). The profile of each component may be computed by applying the Helmholtz free energy minimization criterion to planar surfaces and solving the set of n_c non-linear differential equations in a finite domain[0,L] defined as:

$$\sum_i c_{ij}\frac{d^2\rho_j}{dz^2} = \mu_i\left(\rho_i(z), \ldots\ldots\ldots \rho_n(z)\right) - \mu_i^B \text{ for } i, j = 1 \ldots n_c \quad (15)$$

with$\rho_i(z = 0) = \text{bulk vapor} = \rho_i^V and\ \rho_i(z = L) = \text{bulk liquid} = \rho_i^L$.

4. Result and Discussion

The effect of temperatures and pressures on the IFT of($n-alkane+CH_4$) and ($n-alkane+CO_2$) has been studied.Figure 1-3, the simulated density data[Choudhary et al., 2021] have been compared with the chosen model of DGT+EOS for the ($n-alkane+CH_4$) and ($n-alkane+CO_2$) systems on two isotherms at 323K and 343K and pressure up to 30 MPa. The simulated density data have been fitted as a function of pressure for correlating DGT+EOS for each isotherm with a maximum absolute percentile deviation of 4.0% and average absolute deviation of 1.5%. So, a good agreement between the theory and experiment was found. The simulated IFT data were compared with the predictions using DGT + PR EOS at two isotherms 323K and 343K for pressure up to 30 MPa. Figures 4 - 6give the comparison results of calculated and simulated IFTs data [26] as a function of pressure. It can be seen that the calculated results are in good accordance with the simulated data. The IFTs in these Figures show an opposite dependence on the temperature at lower pressures and positive at higher pressure. The general trend can be observed in each of the plotted graphs.

Error analysis: Interfacial tension determination of three($n-alkane+CH_4$) and three($-alkane+CO_2$) systems have been performed for temperatures at 323K and at 343K and pressure upto 30 MPa for each system. The available simulated data were utilized to meticulously assess the performance of the proposed model by statistical error functions[38], namely Coefficient of Determination(R^2) , Chi-square, Residual Sum of Squares Error(ERRSQ/SSE), Average Relative Error(ARE),Standard Deviation(SD), Mean Square Error(MSE), Root Mean Square Error(RMSE),Percentage Average Relative Deviation (AAD%) and Percentage Absolute Average Relative Deviation(AARD%). The error analysis equations are conveyed as follows:

- Determination Coefficient, a well-known statistical measure that is defined as follows:

$$R^2 = 1 - \frac{\sum_{i=1}^{N}\left(IFT_i^{exp} - IFT_i^{pred}\right)^2}{\sum_{i=1}^{N}\left(IFT_i^{exp} - \overline{IFT}_i^{exp}\right)^2}$$

- Chi-square, it is defined as follows:

$$\text{Chi}-\text{square} = 1 - \frac{\sum_{i=1}^{N}\left(IFT_i^{exp} - IFT_i^{pred}\right)^2}{IFT_i^{exp}}$$

- ERRSQ/SSE, Residual Sum of Square Error is also defined as:

$$ERRSQ/SSE = \sum_{i=1}^{N}\left(IFT_i^{exp} - IFT_i^{pred}\right)^2$$

- ARD, the Average Relative Deviation is defined as:

$$ARE = \frac{1}{N}\sum_{i=1}^{N}\left(\frac{\left(IFT_i^{exp} - IFT_i^{pred}\right)}{IFT_i^{exp}}\right)$$

- ARD%, the Percentage Average Relative Deviation is defined as:

$$ARD\% = \frac{100}{N}\sum_{i=1}^{N}\left(\frac{\left(IFT_i^{exp} - IFT_i^{pred}\right)}{IFT_i^{exp}}\right)$$

- Standard Deviation, a measure indicating the distribution of the values:

$$SD = \sqrt{\frac{1}{N-1}\sum_{i=1}^{N}\left(\frac{IFT_i^{exp} - IFT_i^{pred}}{IFT_i^{exp}}\right)^2}$$

- Mean Square of Error, the average of the squares of discrepancies between the calculated values and the target:

$$MSE = \frac{1}{N}\sum_{i=1}^{N}\left(IFT_i^{exp} - IFT_i^{pred}\right)^2$$

- Root Men Square of Error, the second root of the MSE

$$RMSE = \sqrt{\frac{1}{N}\sum_{i=1}^{N}\left(IFT_i^{exp} - IFT_i^{pred}\right)^2}$$

- Absolute Average Relative Deviation, the absolute average relative AARD:

$$AARD\% = \frac{100}{N}\sum_{i=1}^{N}\left|\left(\frac{\left(IFT_i^{exp} - IFT_i^{pred}\right)}{IFT_i^{exp}}\right)\right|$$

The lower values of the SD, AAD, MSE, RMSE, and AARD, the higher would be the accuracy of the model. The reverse is true in case of the R^2 parameter.R^2: From Table 1-6, Determination coefficient has more value at 443K then at 323K for $C7 + CH_4$ while for $C7 + CO_2$ it is nearly constant. The same was noted for mixtures of all alkanes and natural gases used in this study. So, at higher temperature the accuracy of the model is good. The lower values of standard deviation (SD), average absolute deviation (AAD), mean squared error (MSE), root mean squared error (RMSE), and average absolute relative deviation (AARD) indicate greater accuracy in the model. The opposite is true for the R^2 parameter. According to Table 1-6, the coefficient of determination (R^2) is higher at 443K than at 323K; however, it remains relatively constant at these temperatures. The mixtures of all alkanes and natural gases examined in this study exhibited similar trends at these temperatures. At the elevated temperature of 443K, the model's accuracy is deemed acceptable. Regarding the chi-square analysis, the accuracy of the model is more reliable at 323K compared to 443K, as indicated by the lower value. The same observation has also been noted in the mixtures of all alkanes and natural gases utilized in this study. For the standard deviation (SD), the values are higher at 323K than at 443K. Therefore, the selected model and mixture show better performance at higher temperatures compared to lower temperatures. In contrast, the percentage average relative deviation (ARD%) indicates that the selected model and mixture perform better at lower temperatures. The findings from the study on alkane and natural gas performance reveal a nuanced relationship between temperature and efficiency for these mixtures and the model considered. The performance disparities became more pronounced with temperature variations. Notably, the increased standard deviation at 323K compared to 443K suggests that higher temperatures yield more consistent performance outcomes, which could be advantageous for applications requiring reliability. Conversely, the ARD% metric underscores that these mixtures demonstrate improved efficiency at lower temperatures, highlighting a complex interplay between thermal conditions, model selected and performance metrics.

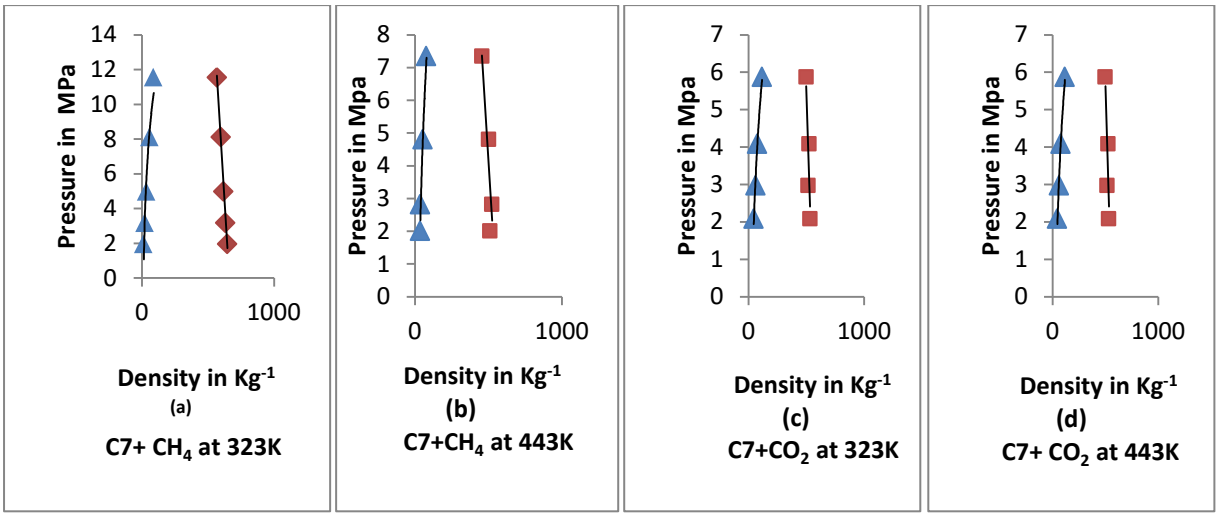

Figure 1 Comparison of predicted density with simulated data[Choudhary et al., 2021] versus pressure P for $C7 + CH_4$ (Figure 1(a) and Figure 1(b))and $C7 + CO_2$ (Figure 1(c) and Figure 1(d)) at 323K and 443K respectively[Choudhary et al., 2021].

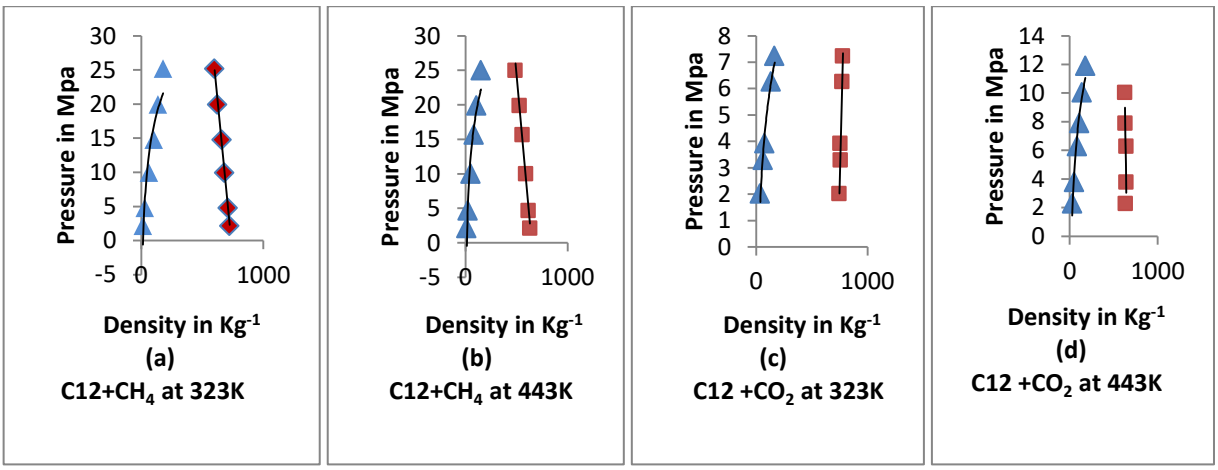

Figure 2 Comparison of predicted density with simulated data[Choudhary et al., 2021] versus pressure P for $C12 + CH_4$(Figure 2(a) and Figure 2(b)) and $C12 + CO_2$(Figure 2(c) and Figure 2(d)) at 323K and 443K respectively[Choudhary et al., 2021].

.

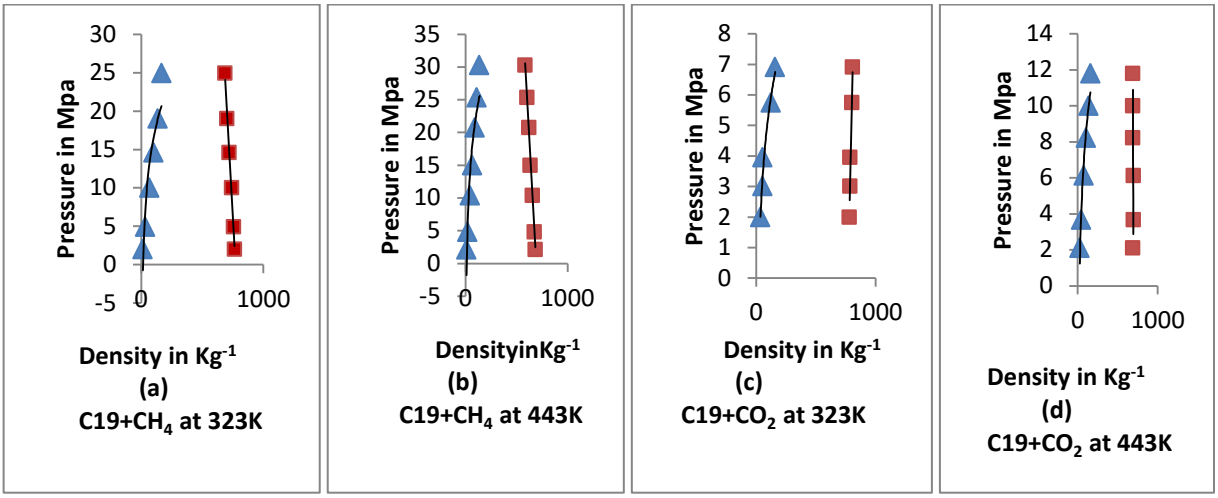

Figure 3 Comparison of predicted density with simulated data[Choudhary et al., 2021] versus pressure P for $C19 + CH_4$(Figure 3(a) and Figure 3(b))and $C19 + CO_2$(Figure 3(c) and Figure 3(d)) at 323K and 443K respectively[Choudhary et al., 2021].

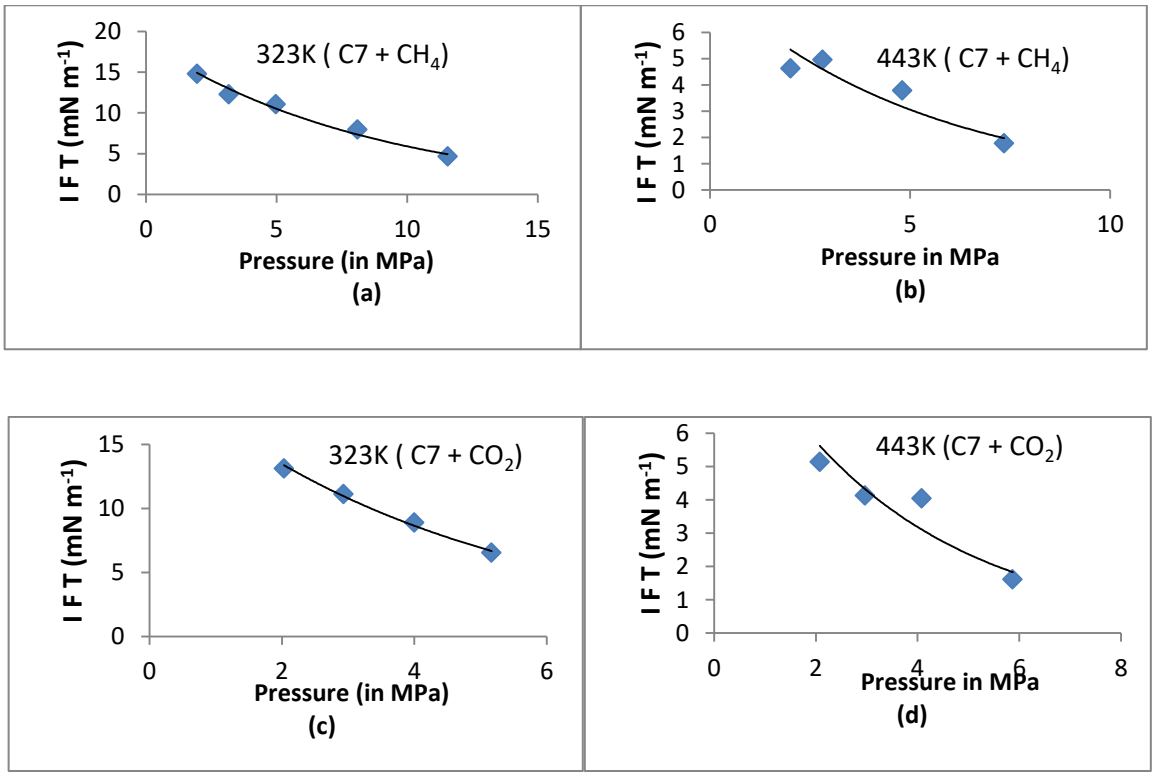

Figure 4:Plot of IFT versus Pressure (a) (C7+CH_4) (b) (C7+CH_4) at323K and 443K, respectively; (c) (C7+CO_2) (d) (C7 + CO_2) at T = 323K and 443K, respectively[Choudhary et al., 2021].

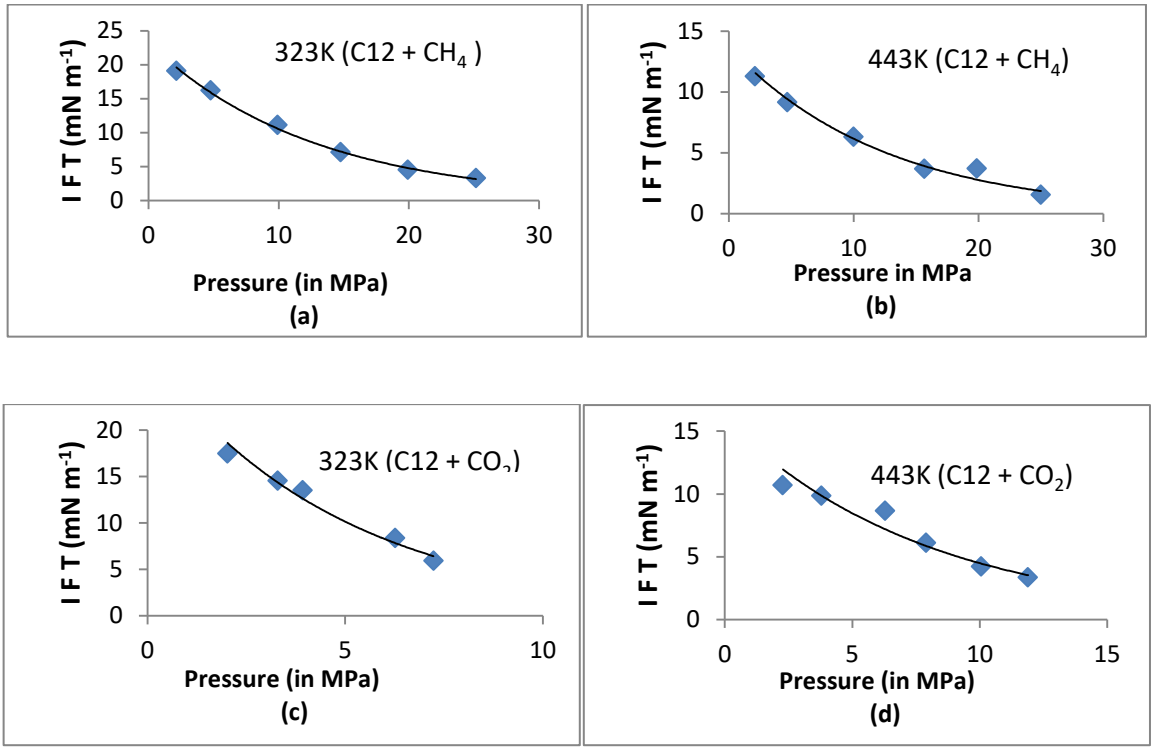

Figure 5:Plot of IFT versus Pressure (a) (C12 + CH_4), (b) (C12 + CH_4) at 323K and 443K, respectively ; (c) (C12 + CO_2), (d) (C12 + CO_2) at T = 323K and 443K, respectively[Choudhary et al., 2021].

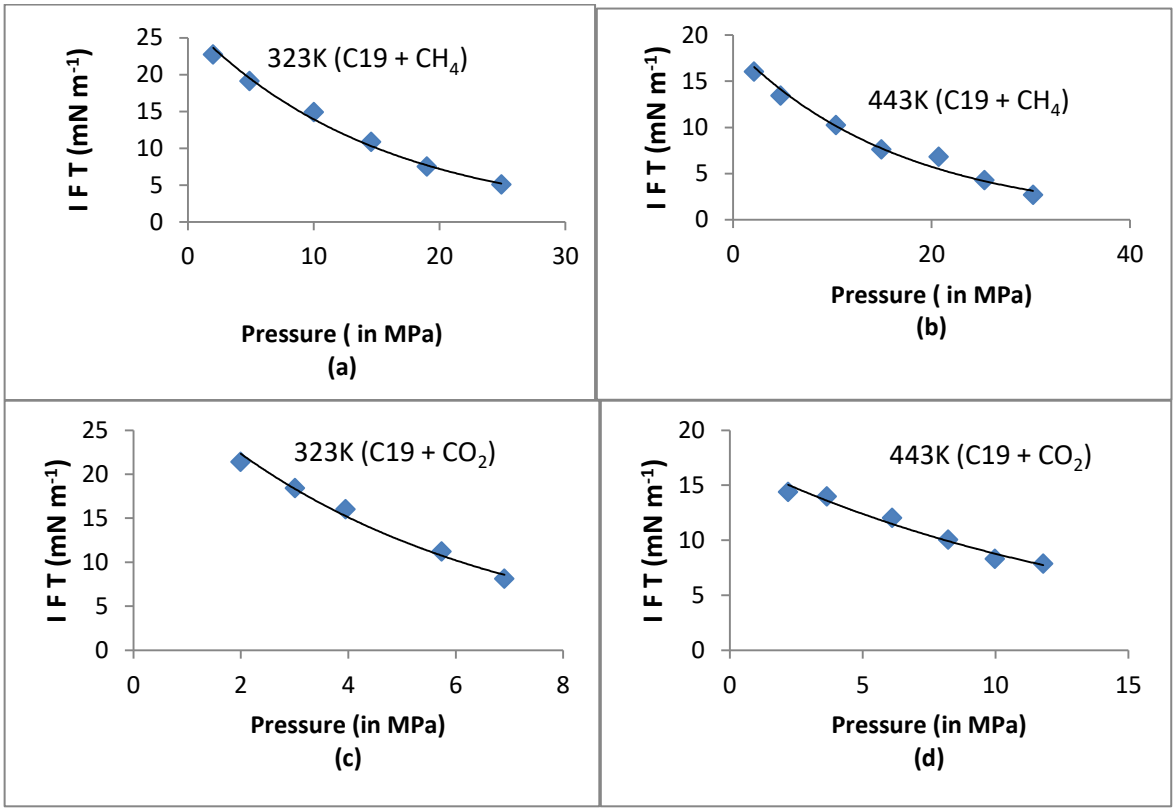

Figure6: Plot of IFT versus Pressure(a)(C19+CH_4),(b)(C19+CH_4)at323K and 443K, respectively; (c)(C19+CO_2), (d) (C19 + CO_2) at T = 323K and 443K, respectively[Choudhary et al., 2021].

Table 1: Pressure with simulated [Choudhary et al., 2021] and calculated IFT Data (this work) and performance evaluation of DGT+EOS for the binary mixture (C7 + CH_4) at 323K and 443K.

$C7 + CH_4$ 323K					$C7 + CH_4$ 443K				
Pressure in MPa	**IFT Expt. mNm^{-1}**	**IFT Calc. mNm^{-1}**	**Residual**	**Residual^2**	**Pressure in MPa**	**IFT Expt. mNm^{-1}**	**IFT Calc. mNm^{-1}**	**Residual**	**Residual^2**
1.953	14.78	14.87	-0.09	0.0081	2.010	4.62	5.36	-0.74	0.5476
3.166	12.27	12.98	-0.71	0.5041	2.813	4.95	4.59	0.36	0.1296
4.972	11.05	10.54	0.51	0.2601	4.804	3.78	3.18	0.60	0.3600
8.103	7.96	7.38	0.58	0.3364	7.349	1.78	1.96	-0.18	0.0324
11.553	4.65	4.94	-0.29	0.0841					
R^2	$Chi.Sq$	$ERSSQ$ or SSE	ARD	SD	R^2	$Chi.Sq$	$ERSSQ$ or SSE	ARD	SD
0.99997	0.126	1.193	-0.1460	12.5311	0.99948	0.258	1.069	-0.7459	4.6168
$\overline{IFT}$ $(Expt.)$	MSE	$RMSE$	ARD%	$AARD$%	$\overline{IFT}$ $(Expt.)$	MSE	$RMSE$	ARD%	$AARD$%
10.1420	0.239	9.7950	914.054	914.054	3.7825	0.2674	3.0517	277.504	277.504

Table 2: Pressure with simulated [Choudhary et al., 2021] and calculated IFT Data (this work) and performance evaluation of DGT+EOS for the binary mixture (C7 + CO_2) at 323K and 443K

$C7 + CO_2$ 323K					$C7 + CO_2$ 443K				
Pressure in MPa	**IFT Expt. mNm^{-1}**	**IFT Calc. mNm^{-1}**	**Residual**	**Residual^2**	**Pressure in MPa**	**IFT Expt. mNm^{-1}**	**IFT Calc. mNm^{-1}**	**Residual**	**Residual^2**
2.031	13.10	13.51	-0.41	0.1681	2.081	5.14	5.86	-0.72	0.5184
2.931	11.10	10.62	0.48	0.2304	2.968	4.13	4.65	-0.52	0.2704
3.998	8.89	7.93	0.96	0.9216	4.084	4.04	3.49	0.55	0.3025
5.167	6.53	5.71	0.82	0.6724	5.870	1.61	2.22	-0.61	0.3721
R^2	$Chi.Sq$	$ERSSQ$ or SSE	ARD	SD	R^2	$Chi.Sq$	$ERSSQ$ or SSE	ARD	SD
0.99987	0.240	1.992	6.1376	13.0737	0.99922	0.472	1.463	-12.7182	4.4517
$\overline{IFT}$ $(Expt.)$	MSE	$RMSE$	ARD%	$AARD$%	$\overline{IFT}$ $(Expt.)$	MSE	$RMSE$	ARD%	$AARD$%
9.9050	0.498	9.2800	896.637	896.637	3.7300	0.3658	2.9650	260.281	260.281

	0								

Table 3: Pressure with simulated [Choudhary et al., 2021] and calculated IFT Data (this work) and performance evaluation of DGT+EOS for the binary mixture (C12 + CH_4) at 323K and 443K.

$C12 + CH_4$ 323K					$C12 + CH_4$ 443K				
Pressure in MPa	**IFT Expt. mNm^{-1}**	**IFT Calc. mNm^{-1}**	**Residual**	**Residual^2**	**Pressure in MPa**	**IFT Expt. mNm^{-1}**	**IFT Calc. mNm^{-1}**	**Residual**	**Residual^2**
2.132	19.07	19.91	-0.84	0.7073	2.114	11.28	12.25	-0.97	0.9409
4.784	16.22	16.11	0.11	0.0121	4.686	9.13	9.69	-0.56	0.3136
9.916	11.12	10.79	0.33	0.1089	10.002	6.29	6.02	0.27	0.0729
14.761	7.12	7.41	-0.29	0.0841	15.674	3.66	3.62	0.04	0.0016
19.934	4.54	4.89	-0.35	0.1225	19.881	3.68	2.47	1.21	1.4641
25.167	3.29	3.25	0.04	0.0016	25.012	1.54	1.56	-0.02	0.0004
R^2	$Chi.Sq$	$ERSSQor SSE$	ARD	SD	R^2	$Chi.Sq$	$ERSSQor SSE$	ARD	SD
0.99998	0.059	1.036	-1.8885	12.0940	0.99991	0.129	2.793	3.7057	6.8209
$\overline{IFT}$ $(Expt.)$	MSE	$RMSE$	$ARD\%$	$AARD\%$	$\overline{IFT}$ $(Expt.)$	MSE	$RMSE$	$ARD\%$	$AARD\%$
10.2265	0.1727	10.9088	920.761	920.761	5.9300	0.4655	5.9711	496.705	496.705

Table 4: Pressure with simulated [Choudhary et al., 2021] and calculated IFT Data (this work) and performance evaluation of DGT+EOS for the binary mixture (C7 + CO_2) at 323K and 443K.

$C12 + CO_2$ 323K					$C12 + CO_2$ 443K				
Pressure in MPa	**IFT Expt. mNm^{-1}**	**IFT Calc. mNm^{-1}**	**Residual**	**Residual^2**	**Pressure in MPa**	**IFT Expt. mNm^{-1}**	**IFT Calc. mNm^{-1}**	**Residual**	**Residual^2**
2.023	17.46	19.42	-1.96	3.8416	2.280	10.70	12.08	-1.38	1.9044
3.290	14.55	14.96	-0.41	0.1681	3.792	9.84	10.07	-0.23	0.0529
3.925	13.49	13.16	0.33	0.1089	6.298	8.64	7.49	1.15	1.3225
6.266	8.37	8.18	0.19	0.0361	7.899	6.11	6.17	-0.06	0.0036
7.233	5.93	6.73	-0.8	0.6400	10.055	4.22	4.78	-0.56	0.3136
					11.898	3.34	3.79	-0.45	0.2025
R^2	$Chi.Sq$	$ERSSQorSS$ 4.794	ARD	SD	R^2	$Chi.Sq$	$ERSSQorSSE$ 0.337	ARD	SD
0.99991	0.243		-4.5635	14.8212	0.99991	0.974		-4.9416	8.3533
$\overline{IFT}$ $(Expt.)$	MSE	$RMSE$	$ARD\%$	$AARD\%$	$\overline{IFT}$ $(Expt.)$	MSE	$RMSE$	$ARD\%$	$AARD\%$
11.9600	0.9589	11.6991	1091.43	1091.436	7.1416	0.6332	6.7102	609.225	609.225

			6						

Table 5: Pressure with simulated [Choudhary et al., 2021] and calculated IFT Data (this work) and performance evaluation of DGT+EOS for the binary mixture (C19 + CH_4) at 323K and 443K.

$C19 + CH_4$ 323K					$C19 + CH_4$ 443K				
Pressure in MPa	**IFT Expt. mNm^{-1}**	**IFT Calc. mNm^{-1}**	**Residual**	**Residual^2**	**Pressure in MPa**	**IFT Expt. mNm^{-1}**	**IFT Calc. mNm^{-1}**	**Residual**	**Residual^2**
2.012	22.73	23.76	-1.03	1.061	2.125	16.04	16.72	-0.68	0.462
4.911	19.08	19.68	-0.60	0.360	4.802	13.42	14.12	-0.70	0.490
10.004	14.87	14.01	0.86	0.739	10.382	10.25	10.08	0.17	0.029
14.570	10.84	10.38	0.46	0.211	14.959	7.62	7.67	-0.05	0.0025
18.988	7.50	7.75	-0.25	0.062	20.738	6.82	5.46	1.36	1.850
24.915	5.05	5.22	-0.17	0.029	25.339	4.27	4.06	0.21	0.044
					30.243	2.68	3.05	-0.37	0.137
R^2	$Chi.Sq$	$ERSSQ$ or SSE	ARD	SD	R^2	$Chi.Sq$	$ERSSQ$ or SSE	ARD	SD
0.99998	0.134	2.463	-0.7247	15.8951	0.99997	0.068	3.014	0.3714	9.9939
$\overline{IFT}$ $(Expt.)$	MSE	$RMSE$	$ARD\%$	$AARD\%$	$\overline{IFT}$ $(Expt.)$	MSE	$RMSE$	$ARD\%$	$AARD\%$
13.3450	0.4105	13.8176	1233.775	1233.775	8.7285	0.4306	8.9212	773.228	773.228

Table 6: Pressure with simulated [Choudhary et al., 2021] and calculated IFT Data (this work) and performance evaluation of DGT+EOS for the binary mixture (C7 + CO_2) at 323K and 443K.

$C19 + CO_2$ 323K					$C19 + CO_2$ 443K				
Pressure in MPa	**IFT Expt. mNm^{-1}**	**IFT Calc. mNm^{-1}**	**Residual**	**Residual^2**	**Pressure in MPa**	**IFT Expt. mNm^{-1}**	**IFT Calc. mNm^{-1}**	**Residual**	**Residual^2**
1.995	21.41	22.38	-0.97	0.9409	2.197	14.38	15.34	-0.96	0.9216
3.006	18.41	18.38	0.03	0.0009	3.661	13.98	13.78	0.20	0.0400
3.95	16.01	15.36	0.65	0.4225	6.115	12.02	11.51	0.51	0.2601
5.739	11.21	10.81	0.40	0.1600	8.227	10.04	9.92	0.12	0.0144
6.906	8.13	8.62	-0.49	0.2401	9.980	8.29	8.74	-0.45	0.2025
					11.795	7.87	7.65	0.22	0.0484
R^2	$Chi.Sq$	$ERSSQ or SSE$	ARD	SD	R^2	$Chi.Sq$	$ERSSQ\ or\ SSE$	ARD	SD

0.99998	0.084	1.764	-0.5532	18.6976	0.99998	0.090	1.487	-0.4066	13.2013
$\overline{IFT}$ $(Expt.)$	MSE	$RMSE$	$ARD\%$	$AARD\%$	$\overline{IFT}$ $(Expt.)$	MSE	$RMSE$	$ARD\%$	$AARD\%$
15.0340	0.3528	14.8280	1402.846	1402.846	11.0967	0.2478	10.4111	1009.260	1009.260

Table 7: Critical properties and acentric factor for alkanes and gases

Component	T_c *(K)*	P_c *(MPa)*	*Acentric Factor*
C7	540.2	2.74	0.350
C12	658.0	1.82	0.576
C19	773.8	1.24	0.853
CH_4	190.6	4.56	0.011
CO_2	304.2	7.29	0.239

5. Conclusion:

This work aimed to enhance the prediction of interfacial tension (IFT) between various n-alkanes and the natural gases methane and carbon dioxide using density gradient theory and an equation of state. The interfacial tension of the CH_4/CO_2-alkane systems is known to diminish with rising pressure. In the case of the IFT-temperature relationship, however, a contradictory trend is observed, in which the IFT decreases or increases with temperature in low and high pressures, respectively. While studying model accuracy analysis, it has been observed that the performance differences increased with temperature. The greater standard deviation at 323K compared to 443K shows that higher temperatures produce more consistent performance, which may benefit reliability-critical applications. The ARD% statistic shows that these combinations are more efficient at lower temperatures, demonstrating a complicated relationship between thermal circumstances, model selection, and performance metrics.

Disclaimer (Artificial Intelligence)

Author(s) hereby declare that NO generative AI technologies such as Large Language Models (ChatGPT, COPILOT, etc) and NO text-to-image generators have been used during writing or editing of this manuscript.

References:

Ameli, F.,Hemmati - Sarapardeh, A., Schaffie, M., Husein, M. M. (2018). Modeling interfacial tension in N2/n alkane systems using corresponding state theory: Application to gas injection processes. Fuel 222 779–791.https://doi.org/10.1016/j.fuel.2018.02.067.

Ashrafizadeh, S.N., Ameri, G.A. (2011). An investigation on the applicability of Parachor model for the prediction of MMP using five equations of state. Chem. Eng. Res. Des. 89, (6), 690–696.https//:doi:10.1016/j.cherd.2010.10.015.

Amar, M., N., Ghriga, M. A., Ben, S.E.A. (2021). Predicting Solubility of Nitrous Oxide in Ionic Liquids Using Machine Learning Techniques and Gene Expression Programming. J. Taiwan Inst. Chem. Eng., 128, 156– 168.https://doi.org/10.1016/j.jtice.2021.08.042.

Amezquita, O.G.N., Enders, S., Jaeger, P.T., Eggers, R.(2010). Evaluation of Interfacial Tension by Image Processing of the Shape Drops J Supercritical Fluids 55 (2) 724–734.http://dx.doi.org/10.1016/j.supflu.2010.09.040.

Blas, F. J., Del Rıo,E. M., De Miguel, E., and Jackson G. (2001). An examination of the vapour-liquid interface of associating fluids using a SAFT-DFT approach. Mol. Phys., 99(22), 1851–1865.Htpps//:doi.org/:10.1080/00268970110075176.

Choudhary, N., NarayananNair, A.K., Che Ruslan,M.F.A., Sun,S. (2019). Bulk and interfacial properties of decane in the presence of carbon dioxide, methane, and their mixture. Sci. Rep. 9, (1), 19784.https://doi:10.1038/s41598-019-56378-y.

Choudhary, N., Ruslan, M.F.A.C., Nair, A.K.N. & Sun, S. (2021). Bulk and Interfacial Properties of Alkanes in the Presence of Carbon Dioxide, Methane, and Their Mixture. Ind.Eng. Chem.Res. 60,729-738.https://doi.org/10.1021/acs.iecr.0c04843.

Cahn, J.W., Hilliard, J.E. (1958). Free energy of a non-uniform system “I” Interfacial free energy. J. Chem. Phys. 28, 258-267.https://doi.org/10.1063/1.1744102.

Carey, B.S., Scriven, L.E., Davis, H.T. (1980). Semi-empirical theory of surface tension of binary systems. AIChE, 26, 5 705-711.https://doi.org/10.1002/aic.690260502.

Guggenheim, E. A. (1945). The Principle of Corresponding States. J. Chem. Phys. 13 (7) 253–261 https://doi.org/10.1063/1.1724033.

Guggenheim, E.A., The Principle of Corresponding States. J.Chem. Phys. 13 (7) 253–261(1945). https://doi.org/10.1063/1.1724033.

Hemmati-Sarapardeh, A., Mohagheghian, E.,(2017), Modeling interfacial tension and minimum miscibility pressure in paraffin-nitrogen systems: Application to gas injection processes. Fuel, 205 80–89. https://doi.org/10.1016/j.fuel.2017.05.035.

Hough, E. W., Stegemeier, G. L. (1961). Correlation of surface and interfacial tension of light hydrocarbons in the critical regionSPE-327-PA1, (04), 259–263,https://doi.org/10.2118/197-PA Jamaloei, B. Y., Kharrat, B., Asghari, K.(2010). Scale events in drainage process through porous media under high and low-interfacial tension flow conditions. J. Pet. Sci. Eng. 75, 223−233. https:// doi.org/10.1016 /j.petrol.2010. 11.006.

Jaeger, P.T., Alotaibi, M.B., Nasr-El-Din, H. A.(2010). Influence of compressed carbon dioxide on the capillarity of the gas− crude oil− reservoir water system.J. Chem. Eng. Data 55, (11), 5246–5251. https://doi:10.1021/je100825b.

Li, X.-S., Liu, J. -M,. Fu, D.(2008). Investigation of Interfacial Tensions for Carbon Dioxide Aqueous Solutions by Perturbed-Chain Statistical Associating Fluid Theory Combined with Density Gradient Theory. Indust. & Engin.Chem Rese. 47, 8911–8917. https://doi.org/10.1021/ie800959h.

Li N., Zhang, C., Ma, Q,L., Jiang L,Y., Xu, Y, X., Chen, C., Sun,Y. L., Yang Y. (2017). Interfacial tension measurement and calculation of (Carbon Dioxide+n-Alkane) binary mixtures. J. Chem. Eng. Data, 62(9), pp.2861-2871.

Lafitte, T., Bessieres, D., Pineiro, M. M., and Daridon, Jean-L.(2006). Simultaneous estimation of phase behavior and second-derivative properties using the statistical associating fluid theory with variable range approach. J. of Chem. Phys., 124, (2), 4509–4524.https://doi.org/10.1063/1.2140276.

Llovell, F., Mac Dowell, N., Blas, F. J., Galindo, A., & Jackson, G.(2012). Application of the SAFT-VR density functional theory to the prediction of the interfacial properties of mixtures of relevance to reservoir engineering. Fluid Phase Equilibria, 336, 137 – 150. https://doi.org/10.1016/j.fluid.2012.07.033.

Mahdaviara, M., Amar, N., Sarapardeh, A. H., Dai,Z., Zhang C., Xiao, T., Zhang, X.(2021). Toward smart schemes for modeling CO_2 solubility in crude oil: Application to carbon dioxide enhanced oil recovery, Fuel 285, 119147.https://doi.org/10.1016/j.fuel.2020.119147.

Mahdaviara, M., Amar, M. N., Ostadhassan, M. &Hemmati-Sarapardeh. (2022). A. On the evaluation of the interfacial tension of immiscible binary systems of methane, carbon dioxide, and nitrogen-alkanes using robust data-driven approaches. *Alex. Eng. J.* 61(12), 11601–11614 https://doi.org/10.1016/j.aej.2022.04.049.

Menad, N.A., Noureddine, Z., Taiwan, J.(2019). An efficient methodology for multi-objective optimization of water alternating CO_2 EOR process. Inst. Chem. Eng. 99, 154–165.https://doi.org/10.1016/j.jtice.2019.03.016.

Mirzaie, M., Tatar, A. (2020). Modeling of interfacial tension in binary mixtures of CH_4, CO_2, and N_2 - alkanes using gene expression programming and equation of state.J.Mol.Liq.320, 114454.https://doi.org/10.1016/j.molliq.2020.114454.

Macleod, D. B. (1923). On a relation between surface tension and density. Trans. Faraday Soc. 19, (July), 38–41.https://doi.org/10.1021/ie50406a015.

Mique, C., Mendiboure, B., Graciaa, A., Lachaise, J.(2008). Petroleum mixtures: An efficient predictive method for surface tension estimations at reservoir conditions. Fuel 87, 612-621.https://doi.org/10.1016/j.fuel.2007.05.049.

Miqueu, C., Mendiboure, B., Graciaa, C., & Lachaise, J.(2004). Modelling of the surface tension of binary and ternary mixtures with the gradient theory of fluid interfaces. Fluid Phase Equilibria, 218, (2), 189–203.https://doi.org/10.1016/j.fluid.2003.12.008.

Miguez,J.M.,Garrido,,J.,M.,Blas,F.J.,Segura,H.,Mejia,A.,Pineiro,M.M.(2014).Comprehensive characterization of interfacial behavior for the mixture CO_2+H_2O+CH_4: Comparison between atomistic and coarse

grained molecular simulation models and density gradient theory. The Journal of Physical Chemistry C, 18, 24504–24519.https://doi.org/10.1021/jp507107a.

Mejıa, A., Segura, H., and Cartes, M. (2011). Measurement and theoretical prediction of the vapor–liquid equilibrium, densities and interfacial tensions of the system hexane + 2-methoxy-2-methylbutane. Fluid Phase Equilibria, 308, (1-2), 15–24. https//doi.org/:10.1016/j.fluid.2011.06.007.

Mejıa, A., Cartes, M., Segura, H., Mu¨ller, E.A., (2014), Use of Equations of State and Coarse Grained Simulations to Complement Experiments: Describing the Interfacial Properties of Carbon Dioxide plus Decane and Carbon Dioxide plus Eicosane Mixtures. J. Chem. Eng. Data 59, (10), 2928–2941.https//:doi:10.1021/JE5000764.

NaitAmar, M., (2020).Modeling solubility of sulfur in pure hydrogen sulfide and sour gas mixtures using rigorous machine learning methods. Int. J. Hydrogen Energy 45 (58) 33274–33287https://doi.org/10.1016/j.ijhydene.2020.09.145.

NaitAmar, M., Ghriga, M. A., Ouaer, H. (2021). On the evaluation of solubility of hydrogen sulfide in ionic liquids using advanced committee machine intelligent systems. J. Taiwan Inst. Chem.Eng. 118, 159–168.https//:doi.org:/ 118 (2021) 159168.

Pereira, L.M.C., Chapoy, A., Burgass, R., Oliveira, M.B., Coutinho, J.A.P., Tohidi, B. (2016). Study of the impact of high temperatures and pressures on the equilibrium densities and interfacial tension of the carbon dioxide/water system. J. Chem. Thermodyn. 93, 404–415.https://doi.org/10.1016/j.jct.2015.05.005.

Reno, G. J., Katz, D.L. (1943). Surface tension of n-heptane and n-butane containing dissolved nitrogen. Ind. Eng. Chem. 35, (10), 1091–1093.

Sugden, S. J.(1924). The variation of surface tension with temperature and some related functions. J. chem. Soc. Trans.125, (0), 32–41.https://doi.org/10.1039/CT9242500032.

Sahimi, M. and Taylor, B. N. (1991). Surface Tension of Binary Liquid-Vapor Mixtures: A Comparison of Mean-Field and Scaling Theories," Journal of Chemical Physics 95, 6749-6761.https://doi.org/10.1063/1.461514.

Sarapardeh, A. H., Varamesh, A., Husein, M.M., Karan, K. (2018). On the evaluation of the viscosity of nanofluid systems: Modeling and data assessment," Sustainable Energy Reviews, Elsevier, vol. 81(P1), pages 313-329. https://libkey.io/10.1016/j.rser.2017.07.049.

Weinaug, C. F., Katz, D.L.(1943). Surface Tension of Methane-Propane Mixtures. Industrial Engineering Chem 35, 2, 239–246.https://doi.org/10.1021/ie50398a028.

Warsito, B., Santoso, R., Suparti., Yasin, H.(2018). Cascade Forward Neural Network for Time Series Prediction. J Phys. Conf. Ser.1025, 012097.https//: doi.org/10.1088/1742-6596/1025/1/012097.

Zolghadr, A., Escrochi, M., Ayatollahi, S. (2013). Temperature and Composition Effect on CO2 Miscibility by Interfacial Tension Measurement. J. Chem. Eng.Data 58, (5), 1168–1175.https://doi.org/10.1021/je301283e.

Zuo,Y.-X., Stenby, E. H. (1996). Calculation of Surface Tensions of Polar Mixtures with a Simplified Gradient Theory Model. J. Chem. Eng. Jpn. 29, (1), 159–165. https://doi.org/10.1252/jcej.29.159.